A novel plant actin-microtubule bridging complex regulates cytoskeletal and ER structure at ER-PM Contact Sites

Jingze Zang[1,2,3,7], Sandra Klemm[4,7], Charlotte Pain[5], Patrick Duckney[3], Zhiru Bao[1,2], Gina Stamm[4], Verena Kriechbaumer[5], Katharina Bürstenbinder[4], Patrick J Hussey[3,6]* and Pengwei Wang[1,2,8]*

1. Key Laboratory of Horticultural Plant Biology (MOE), College of Horticulture and Forestry Sciences, Huazhong Agricultural University, Wuhan 430070, Hubei Province, China; 2. Interdisciplinary Sciences Research Institute, Huazhong Agricultural University, Wuhan, 430007, China; 3. Department of Biosciences, Durham University, South road, Durham, DH1 3LE, UK; 4. Department of Molecular Signal Processing, Leibniz Institute of Plant Biochemistry, D-06120 Halle, Germany; 5. Plant Cell Biology, Oxford Brookes University, Oxford, OX3 0BP, UK; 6. Department of Experimental Plant Biology, Charles University, Faculty of Science, Viničná 5, CZ 128 43 Praha 2, Czechia

7. These authors contributed equally to this work
8. Lead Contact
*Corresponding author: wangpengwei@mail.hzau.edu.cn; p.j.hussey@durham.ac.uk

Summary

In plants, the cortical ER network is connected to the plasma membrane through the ER-PM contact sites (EPCSs), whose structures are maintained by EPCS resident proteins and the cytoskeleton [1-7] . Strong co-alignment between EPCSs and the cytoskeleton are observed in plants [1, 8], but little is known of how the cytoskeleton is maintained and regulated at the EPCS. Here we have used a yeast-two-hybrid screen and subsequent *in vivo* interaction studies in plants by FRET-FLIM analysis, to identify two microtubule binding proteins, KLCR1 (Kinesin Light Chain Related protein 1) and IQD2 (IQ67-Domain 2) that interact with the actin binding protein NET3C and form a component of plant EPCS, that mediates the link between the actin and microtubule networks. The NET3C-KLCR1-IQD2 module, acting as an actin-microtubule bridging complex, has a direct influence on ER morphology and EPCS structure. Their loss of function mutants, *net3a*/NET3C RNAi, *klcr1* or *iqd*2, exhibit defects in pavement cell morphology which we suggest is linked to the disorganization of both actin filaments and microtubules. In conclusion, our results reveal a novel cytoskeletal associated complex, which is essential for the maintenance and organization of cytoskeletal structure and ER morphology at the EPCS, and for normal plant cell morphogenesis.

Keywords: NET family, kinesin-light-chain-related-proteins, IQD family, ER-PM contact sites, ER network, plant cell morphogenesis

Results and Discussion

Kinesin-light chain related protein (KLCR) interacts with NET3C

NETWORKED 3C (NET3C) belongs to a plant specific NETWORKED superfamily of actin binding proteins[9], it localizes at the EPCSs and interacts with the ER localized vesicle-associated membrane protein (VAMP)-associated protein 27 (VAP27) proteins and the cytoskeleton[1, 8]. In order to characterize the function of NET3C, a yeast-two-hybrid screen was performed using NET3C as bait, which identified an interaction with KLCR1 (also known as Cellulose synthase-microtubule Uncoupling 1) that associates with microtubules and the plasma membrane (Figure 1A) [10-12]. In Arabidopsis, KLCR1 has two close homologues (Figure 1B). One-on-one yeast-2-hybrid (Y2H) interaction tests were performed between the NET3 and KLCR families. The results indicate that NET3C interacts with all three KLCR proteins, while NET3A exhibits weak interactions with KLCR1/2 (Figure 1C), suggesting some redundancy in their interactions.

To further investigate the NET3C-KLCR interaction, *in vivo* colocalization analyses were performed. In *N. benthamiana* leaf epidermal cells, Red fluorescent protein (RFP)-NET3C can recruit KLCR1/2-Green fluorescent protein (GFP) to the EPCSs from the cytoplasm, but not KLCR3 (Figures 1D-1G). The effectiveness of NET3C recruitment was measured using the signal intensity ratio; the strongest recruitment was seen with KLCR1 (Figure 1H). In agreement with the yeast two hybrid and co-localization results, the interaction between NET3C and KLCR1/2/3 was further tested in a FRET-FLIM assay [13]. The average fluorescence lifetimes of GFP-NET3C were reduced significantly in the presence of RFP-tagged-KLCRs indicating physical interactions. The negative control using free RFP is not able to reduce the lifetime of GFP-NET3C (Figures 1I-1J).

Taken together, we have identified an interaction between NET3C and KLCR1. Having such an interaction would enable KLCR1 to be recruited to VAP27/NET3C labelled EPCSs.

KLCR1 forms stationary foci that associate with microtubules, ER and NET3C at endogenous conditions.

Analysis of subcellular KLCR1-GFP localization expressed in Arabidopsis under normal endogenous conditions (driven by its native promoter) revealed that KLCR1-GFP forms stationary puncta that associate with cortical microtubules in a beads-on-a-string pattern (Figure 2A-2C). Some of these KLCR1 foci also associated with the ER; kymograph analyses indicate that these structures are relatively immobile and that they closely associate with

stationary ER structures, a feature that is reminiscent of ER-PM contact sites (Figure 2D-2E).

Immunofluorescence studies were also performed using the transgenic *pKLCR1*:KCLR1-GFP (*klcr1*) line and a NET3C antibody [1]. As expected, endogenous NET3C localizes to EPCSs that are associated with the ER network (Figure 2F). Partial co-localization/co-alignment between endogenous NET3C and KLCR1-GFP labeled microtubules is observed (Figure 2G, arrow), suggesting that these KLCR1 puncta associated with ER and NET3C at the EPSCs. As a control, the NET3C antibody was pre-incubated with a NET3C peptide before immuno-labeling and this resulted in the NET3C signal being almost completely abolished, indicating the effectiveness of the NET3C antibody (Figure 2H). Taken together, the co-localization results between anti-NET3C and ER; anti-NET3C and KLCR1-GFP, further support the conclusion that the KLCR1 labelled foci are EPCS associated.

All three KLCRs associate with microtubules through IQ67 domain proteins (IQD)

Previous studies reported that KLCR1 locates to microtubules through IQD proteins, which are plant-specific proteins that bind to calmodulin [10, 11]. The IQD protein family has 33 members, most of them are localize to microtubules and regulate plant development [14-16]. Some IQD proteins (e.g., IQD13), are also able to associate with the plasma membrane and act as a lateral fence to spatially control the plasma membrane domains [17].

In this study, we further demonstrate that KLCR proteins can be recruited to microtubules through their interaction with IQD2 (Figure S1). When RFP tagged KLCR proteins are expressed alone in *N. benthamiana*, they show a cytosolic localization (Figures S1A-S1C). However, when they are co-expressed with GFP-IQD2, they can be clearly seen on the microtubules (Figures S1D-S1G).

Upon strong expression (e.g., using the 35S promoter), KLCR proteins localize to the cytosol, indicating that the amount of endogenous IQD protein is too low to efficiently recruit large amounts of KLCR proteins to microtubules; the cytoplasmic background is also likely to mask any observable weak microtubule labeling. This phenomenon is similar to the localization patterns observed with TONNEAU 1 (TON1) which also localizes to the cytosol in tobacco cells but can be targeted to microtubules in the presence of TON1 Recruiting Motif (TRM) proteins [18, 19]. However, when there is weak expression of KLCRs under the control of a ubiquitin promoter in *N. benthamiana,* co-alignment of KLCRs with microtubules is also observed (Figure S1H), like what is shown in stable transgenic lines.

The NET3C-KLCR-IQD complex exists in plants

As KLCR proteins are recruited to microtubules by proteins from the IQD family (Figure 2 and Figure S1), and KLCRs interact with NET3C at the ER-PM contact sites, we asked whether NET3C could also interact with IQDs to form a trimeric NET3C-KLCR-IQD complex, using the split-ubiquitin system [20]. We observed no direct interaction between NET3C and IQD2 in this assay, but the interaction between KLCR1 and NET3C, and between KLCR1 and IQD2 was consistently reproducible (Figure 3A). Interestingly, when either KLCR1 or KLCR2 is included, interactions between NET3C and IQD2 are clearly identified (Figure 3B). Furthermore, almost complete co-localization was observed when these three proteins are co-expressed *in vivo* (Figure 3C).

In agreement with this result, we found that if the expression level of IQD2 is low, partial association between NET3C, IQD2 and microtubules is seen (Figure S2A), and the co-localization between NET3C and IQD2 can be enhanced in the presence of KLCR1 (Figure S2B). A strong association between NET3C and IQD2 is achieved when the expression levels of both NET3C and IQD2 are high (Figure S2C). It is likely that NET3C and IQD2 may exhibit indirect or a very weak association, and KLCR acts as a 'linker/stabilizer' between NET3C and IQD2, facilitating the interaction. Similarly, partial co-localization between GFP-IQD2 and endogenous NET3C is found in Arabidopsis cells that are immuno-labelled with the NET3C antibody (Figure S2D), whereas, strong co-localization of IQD2 and NET3C can be achieved in Arabidopsis cells transiently over-expressing these proteins (Figure S2E). FRET-FLIM studies indicate that the fluorescence lifetime of GFP-NET3C is not affected dramatically when co-expressed with RFP-IQD2(despite strong co-localization), supporting the fact that these two proteins are part of a complex but do not directly interact (Figure 3D).

Moreover, when NET3C is co-expressed with other IQD proteins, clear co-localization can be observed with IQD1, IQD12 and IQD22, but not with IQD25 (Figure S2F-S2G), suggesting that the complex of NET3C and IQDs exist across the different IQD subgroups. In summary, we have demonstrated the existence of a novel protein complex consisting of NET3C-KLCRs-IQD2 that crosslink actin and microtubules at the ER and PM interface [1, 10, 14](Figure 3E and 3F).

NET3C-KLCR1-IQD2 complex mediates the interaction between actin, microtubules and ER at the EPCS

It has been shown that alteration in EPCS has a direct effect on the morphology of the ER. For example, wider ER polygonal structures are observed in Arabidopsis *syt1* knock-out mutants

[2]. Moreover, ionic stress can redistribute SYT1 along cortical ER tubules and increases the number of EPCS, thereby increasing ER-PM connectivity [3]. NET3C is a plant specific protein that mediates the link between the ER and the PM [1]. Therefore, altering the abundance and localization of NET3C may be predicted to have a direct impact on the morphology of the ER network. Indeed, the number of fully enclosed ER polygons is significantly increased in cells overexpressing NET3C (p=9.1815e-04) (Figure 3G-I). This is likely to be because NET3C overexpression results in the generation of additional ER-PM contact sites, thereby increasing the number of ER polygons (Figure 3J).

Endogenous NET3C localizes to discrete punctate structures which are closely associated with the ER network and KLCR1/IQD2 labelled microtubules (Figures 2F-G and S2D). Interestingly, when both RFP-NET3C and GFP-IQD2 are co-expressed in *N. benthamiana*, the overall ER network follows the same pattern as the microtubules (Figure 3K). Strong ER-microtubule co-alignment is found in cells co-expressing NET3C, IQD2 and VAP27-1; with NET3C/VAP27-1 labeled EPCSs appearing as puncta aligning along IQD2 labeled microtubules (Figure 3L). Therefore, the rearrangement of the ER network along microtubules is likely to be due to an increased ER-microtubule association, and the altered distribution of EPCSs (Figure 3M). In addition, some triple transient expression studies have been performed as controls: NET3C, KLCR1 and VAP27-1 (Figure S3A); NET3C, KLCR1 and HDEL (Figure S3B); IQD2, KLCR1 and VAP27-1 (Figure S3C). None of these combinations exhibit strong ER-microtubule co-alignment as observed in Figure 3K. However, the overexpression of KLCR1 and IQD2 can also lead to partial co-alignments of microtubules and ER tubules (Figure S3D), although not as strong as overexpression of IQD2 and NET3C. We therefore hypothesize that KLCR1 can serve as a bridge between IQD2 and NET3C and the co-existence of NET3C, VAP27, KLCR1 and IQD is important for mediating the interaction between ER-PM and the cytoskeleton.

As KLCR1 and IQD2 have been shown to localize to microtubules, and NET3C is known to bind the actin, then the NET3C-KLCR1-IQD2 complex could mediate the link between the two filament systems at the EPCS. To test this hypothesis, Yellow fluorescent protein (YFP)-actin-Chromobody (Actin-Cb) or Kinesin Motor Domain (KMD)-RFP were co-expressed with both IQD2 and NET3C in *N. benthamiana*. CFP-IQD2 co-localized with RFP-NET3C on KMD-GFP labeled microtubules (Figure S3E) or YFP-Actin-Cb labeled actin filaments (Figure S3F). Cells expressing both YFP-Actin-Cb, KMD-RFP and HDEL were used as a control and no co-alignment between actin filaments, microtubules and ER network was observed (Figure S3G).

It is known that the ER dynamics in plants is also regulated by microtubules [21, 22]. As the

NET3C-KLCR1-IQD2 complex can mediate the connection between actin filaments and microtubules, this indicatesplants may have a specific mechanism for enabling actin-microtubule and ER interactions. Furthermore, enhanced association of ER and the cytoskeleton is found when NET3C-KLCR-IQD2 were over-expressed (Figure 3C, K-L) which is in agreement with our conclusion that these proteins have the capability to mediate the link between ER and the cytoskeletal network (Figure 3E-F). However, when these proteins are kept at endogenous levels, the complex is likely localized to the place where ER, PM, actin and microtubules normally converge, that is at the EPCS (Figure 3M) [8].

The structures of ER/EPCS and the cytoskeleton are affected when the NET3C-KLCR1-IQD2 complex is dysfunctional.

In order to study the function of the NET3C-KLCR1-IQD complex in plants, we used T-DNA insertion mutants of *klcr1* (the key component of the complex) (Figure S4A-B), and crossed them with MAP4-GFP/Tubulin-mCherry (microtubules) and Lifeact-GFP (Actin) Arabidopsis reporter lines. Clear disorganization of the cytoskeletal network is observed in the *klcr1* mutants (Figure 4A-B). The microtubule fibril array anisotropy score was used to assess microtubules organization, the score is from 0 (no order) to 1 (ordered) [23]. The average anisotropy score in wild type cells is significantly higher than that in *klcr1* mutants, indicating that the microtubule arrays in cotyledon pavement cells of *klcr1* are less ordered (Figure 4C-D). Mutants carrying the actin marker appeared to have fewer weakly labeled thin filaments and more thick bundled filaments (Figure 4E). The skewness of fluorescence intensity distribution was used to investigate the level of actin filament bundling. The average skewness value of actin filaments in wild type plants was significantly smaller than the value in the same cells in *klcr1* plants (Figure 4F). Such a cytoskeletal phenotype is also reported in other *iqd* mutants (e.g., *iqd5*) [15], so it is likely that the *iqd2* mutant in this study exhibits similar defects.

Moreover, the EPCS marker VAP27-1-YFP was also crossed into *klcr1* mutants. We observed that the ER structure is affected in the *klcr1* mutant; the area of ER cisternae increased significantly as quantified using “AnalyzER” (Figure 4I-J). In plants co-expressing VAP27-1-YFP and Lifeact-GFP, co-localization between thick ER streaming and actin bundles is prominent, and such an arrangement is rarely observed in wild type plants (Figure 4G-H). Interestingly, the size of VAP27 labelled EPCSs appear much smaller (Figure 4I-K). Taken together, these data suggest that the NET3C-KLCR1-IQD complex is essential for EPCS structure. Previous studies have indicated that microtubules are essential for EPCS-VAP27 protein dynamics [1], which likely involves the function of microtubule-localized proteins at the EPCS (e.g., KLCR1).

Arabidopsis mutants of NET3C, KLCR1 and IQD2 are defective in cell expansion and pavement cell morphogenesis.

When *klcr1* and *iqd2* seedlings were grown on vertical plates, the overall development appears similar to wild type, however, their roots skewed to the left (Figure 4L-M). This phenotype is likely due to the left-handed helical arrangement of the root epidermal cells (Figure 4N), a phenomenon that has been reported in plants with aberrant microtubule organization [24-26]. Expression of *proKLCR1*:KLCR1-GFP or *proIQD2*:IQD2-GFP in their respective mutant plants was able to rescue the twisting root growth phenotype (Figure 4L-N), suggesting that the phenotype of *klcr1* and *iqd2* is directly related to the loss-of-function of KLCR1 or IQD2.

Furthermore, quantitative analysis (using PaCeQuant [27]) suggests that the morphogenesis of leaf pavement cells is also significantly altered. In wild type plants, cotyledon pavement cells show an interlocking jigsaw puzzle appearance with lobes and indentations. However, in both the *klcr1* and the *iqd2* mutants, the cells became more circular, and other key parameters such as average lobe length and the max core width of the pavement cells are also significantly changed (Figure 4O-P). Moreover, pavement cell morphology in the *net3a*/NET3C RNAi mutant was also studied, as our result showed that NET3A and NET3C are likely to interact with KLCR proteins (Figure 1C). The leaf pavement cells from these double mutants also exhibit a small but significant difference in cell area and circularity (Figure S4C-D). Taken together, we suggest that disruption of the protein composition of the NET3C-KLCR1-IQD complex has an overall effect on cell morphology.

Some cytoskeletal associated proteins localize to the membrane-cytoskeleton interface [28, 29], where membrane remodeling could possibly interplay with cytoskeletal organization thereby regulating key subcellular activities. Members of the KLCR and IQD families are known as PM peripheral associated proteins from previous studies [11, 14]. Here we have demonstrated that these proteins can interact with NET3C, forming a NET3C-KLCR-IQD complex at the ER-PM interface where the actin cytoskeleton and microtubules converge. These findings support our hypothesis that EPCS in plants may act as a hub for cytoskeletal organization and signal sensing [30]. In the wild type, some actin cytoskeleton may cross-link with microtubules at the EPCS [1, 8] through the NET3C-KLCR1-IQD2 complex. The loss of function of KLCRs affects the association between NET3C and IQDs at the actin, microtubule and EPCS interface, resulting in changes in cytoskeletal and ER organization (Figure 4Q).

KLCR1 is known to stabilize microtubules at the cell cortex [11, 12], whether this process

involves EPCS remains to be confirmed. In plants with a dysfunctional NET3C-KLCR-IQD complex, the ER, EPCS structure and cytoskeletal organization are altered. Consequently, a defective developmental and cell morphology phenotype is observed. However, with the tools we have to date, it is impossible to tell whether the mutant phenotype is a direct effect of cytoskeletal rearrangement, or ER/EPCS alteration. As the cytoskeleton-ER system are closely linked, affecting one component is likely to have a direct effect on the other. In previous work, IQD proteins have been shown to interact with calmodulin, which may suggest that the activity of the NET3C-KLCR1-IQD2 is mediated by a calcium signal. Such calcium signals could be sensed by IQDs through their interaction with calmodulin, consequently changing cytoskeletal and ER organization in that region. This could be important as the degree of ER-PM connection has a direct effect on exocytosis, endocytosis, autophagy and lipid transport [31-36].

Acknowledgements

We thank Jinli Gong, Johan Kroon for their help in this work. We also appreciate the assistance from Xiaolu Qu and the microscopy core facilities of the College of Horticulture & Forestry sciences, Huazhong Agricultural University. The project was supported by NSFC grants (no. 91854102), Fundamental Research Funds for the Central Universities (2662018PY010), HZAU Scientific & Technological Self-innovation Foundation (2017RC004) and Thousand Youth Talents Plan Project to P.W; and a BBSRC grant (BB/G006334/1) to P.J.H, and by GIF grant (no. G-1482-423.13/2018) and core funding of the Leibniz Association to K.B.

Author Contribution

P.W. and P.J.H. conceived and supervised the project, J.Z. and S.K. perform most of the experiments. J.Z, K.B., P.J.H. and P.W. wrote the manuscript. C.P. and V.K. performed the ER morphology analysis. K.B. and S.K. provided the IQD constructs and Arabidopsis lines; P.D., Z.B. and G.S. helped with confocal imaging, material preparation and data interpretation.

Declaration of Interests

The authors declare no competing interests.

Main Figures

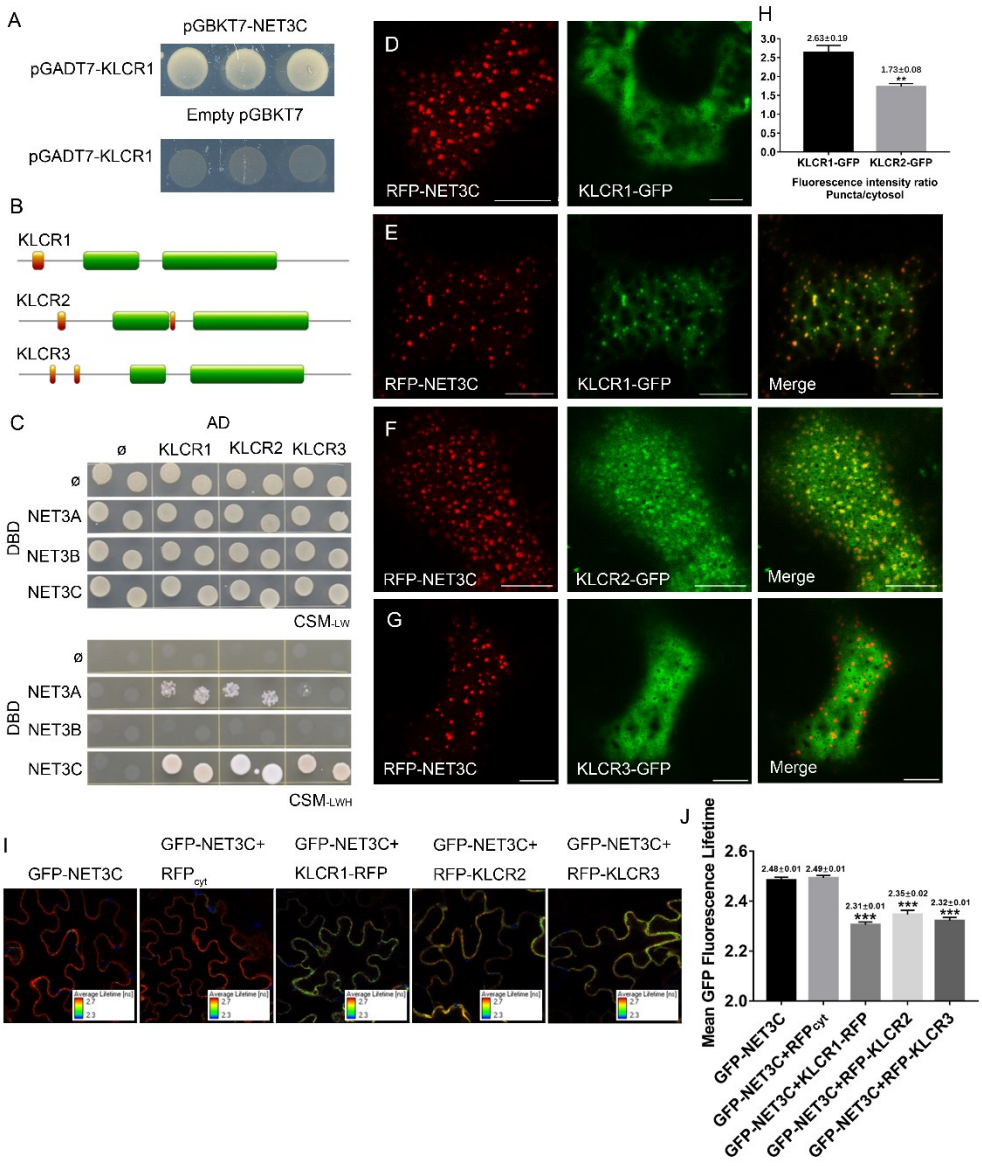

Figure 1. NET3C interacts with KLCR proteins. (A) The interaction between full length NET3C and KLCR (a.a.11-269) was identified in a Y2H screen. **(B)** Predicted protein structures of KLCR proteins in Arabidopsis using the Simple Modular Architecture Research Tool (SMART) program. Green boxes indicate tetratricopeptide regions (TPR), which from a right-handed helical structure serves as a platform to facilitate protein-protein interactions; red boxes indicate regions of low complexity and grey lines represent non-domain containing protein regions. **(C)** Y2H assay of interactions between NET3 proteins and full length KLCR proteins. Growth assay of haploid yeast cells co-expressing GAL4-DNA Binding Domain (DBD) fusions of NET3A, NET3B and NET3C with GAL4-Activation Domain (AD) fusions of KLCR1, KLCR2 and KLCR3. DBD and AD alone (ø) were included as negative controls. Yeast cells were grown for 2 days on vector-selective media (Complete Supplement Mixture [CSM]-Leucine, Tryptophan [LW]) and on interaction-selective media (CSM-Leucine, Tryptophan, Histidine [LWH]). **(D)** The

subcellular localization of NET3C and KLCR1 in *N. benthamiana* leaf tissues. NET3C and KLCR1 are localized at the punctate structures and in the cytosol, respectively, when they are expressed on their own. **(E-H)** The expression of RFP-NET3C can recruit KLCR1-GFP and KLCR2-GFP to punctate structures, but not KLCR3-GFP. The fluorescence intensity of the KLCR1/KLCR2-GFP cytosolic background and puncta werecalculated using image J. Asterisks indicate statistically significant differences from wild type (Student's t-test, **p<0.01). n=5 cells. **(I-J)** FRET-FLIM analysis of the interactions between NET3C, KLCR1, KLCR2 and KLCR3. The average fluorescence lifetime of GFP-NET3C when expressed on its own was found to be 2.48±0.01 ns, whereas the average fluorescence lifetime of GFP-NET3C was reduced by 0.17, 0.13 and 0.16 ns when co-expressed with KLCR1, KLCR2 and KLCR3 respectively. GFP-NET3C was co-expressed with RFP_{cyto} as a negative control and the fluorescence lifetime was measured at 2.49±0.01 ns. Asterisks indicate statistically significant differences from wild type (t-test, ***p<0.001). Scale bar: 10 μm. See also Figure S1.

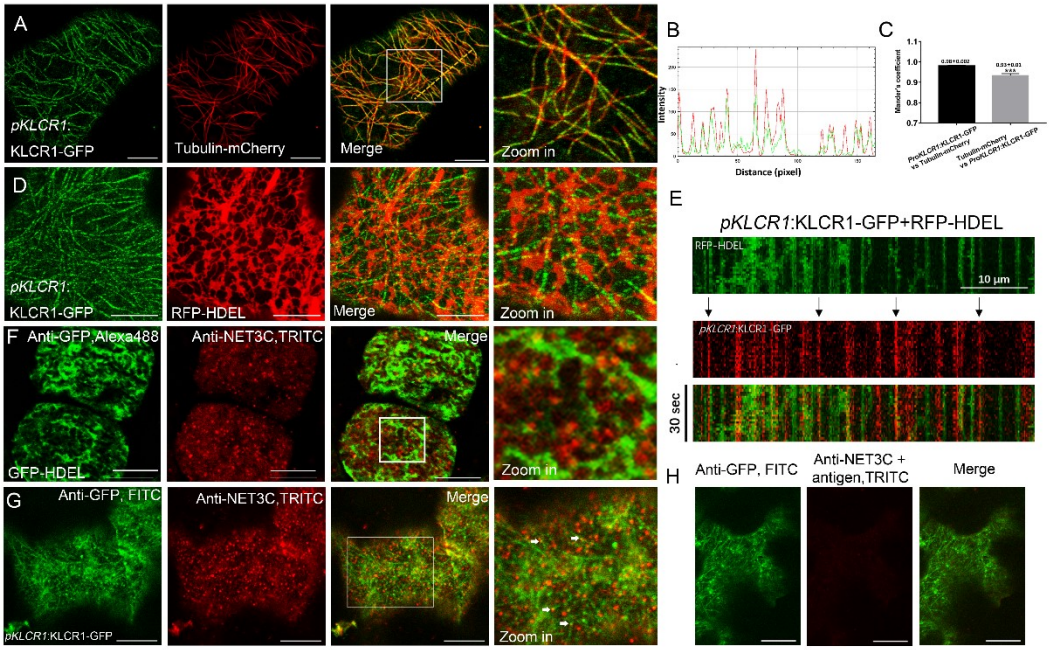

Figure 2. KLCR1 is associated with microtubules, ER and NET3C at the endogenous conditions. **(A)** KLCR1 in Arabidopsis forms foci which co-localized with microtubules. **(B)** Fluorescence intensity plot along the dashed line in (A) (merge). The picks of KLCR1 and Tubulin signals were highly corelated. (**C)** Mander's coefficient test of KLCR1-GFP and Tubulin-mCherry co-localization in Arabidopsis cotyledon cells. The coefficient of the KLCR1-GFP against the Tubulin-mCherry is significantly higher than the reverse, indicating that not all of the microtubules were covered by KLCR1 signals. Asterisks indicate statistically significant differences from wild type (t-test, ***p<0.001)**.** n=16 cells form 5 seedlings. **(D)** Most of the KLCR1 foci are associated with the ER network. **(E)** Association of KLCR1 with the ER network further corroborated by a kymograph. The black arrows indicate the stable association sites. **(F)** Immunofluorescence of GFP-Histidine, aspartic acid, glutamic acid, Leucine (HDEL) expressing Arabidopsis root tips with GFP and NET3C antibodies. Endogenous NET3C forms puncta which were associated with the ER network. **(G)** Immunofluorescence of *pKLCR1*:KLCR1-GFP expression Arabidopsis cotyledon epidermal cells with GFP and NET3C

antibodies. Some NET3C puncta co-aligned with KLCR1 labeled microtubules and co-localized with KLCR1 foci (59.3±0.1% association); white arrows indicate examples of co-alignment and association. n=5 cells. **(H)** Co-incubation of the NET3C peptide immunogen with the NET3C antibody before immune-labeling. The NET3C signal seen previously was abolished with no effect on the KLCR1 labelling of the microtubules. Scale bar: 10 μm.

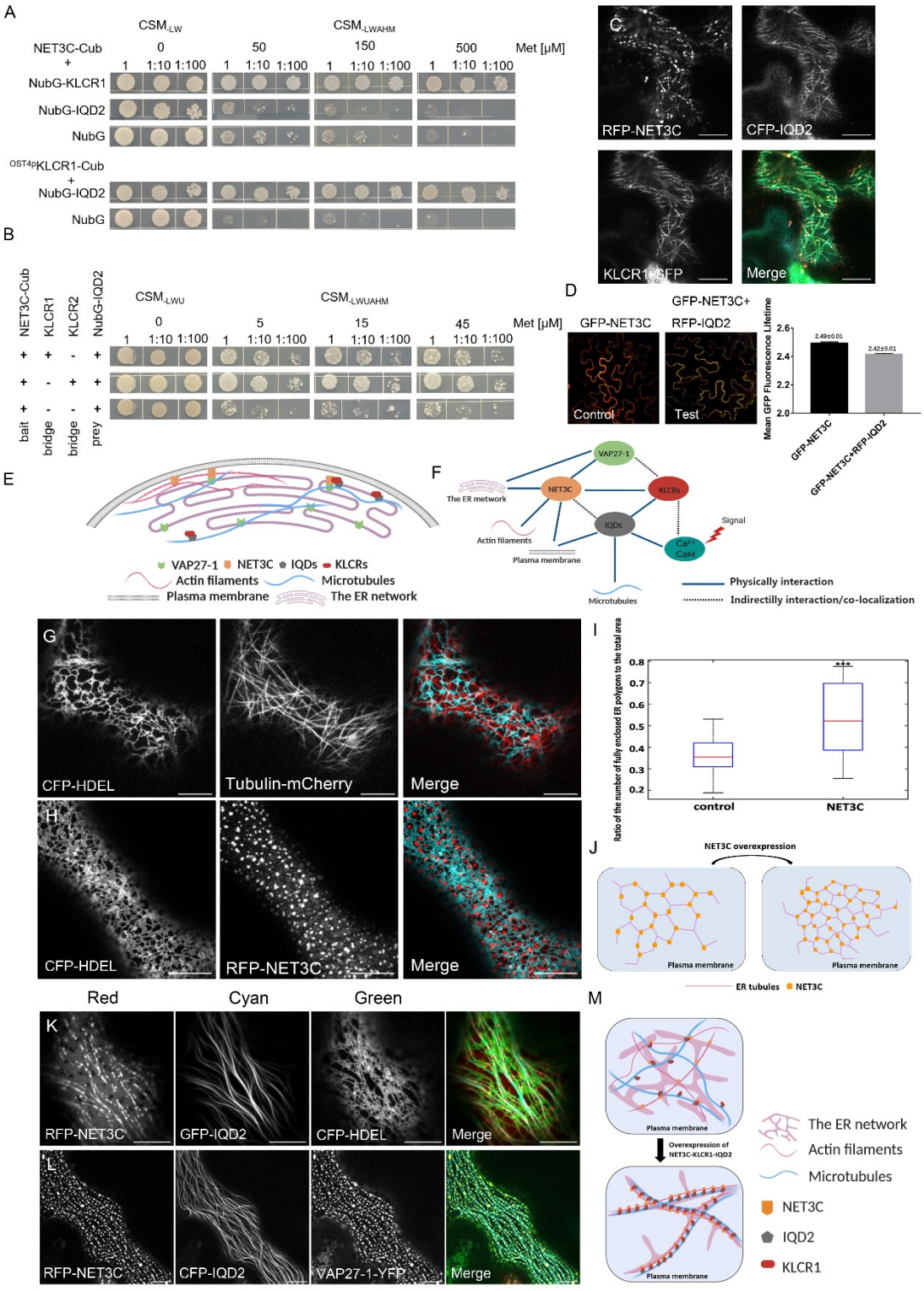

Figure 3. NET3C forms a complex with KLCR1 and IQD2, mediating the interaction between actin, microtubules and ER at the EPCS. (A) Growth assay of haploid yeast cells co-expressing NET3C-Cub with NubG-fusions of KLCR1 and IQD2 (top); KLCR1-Cub with NubG-IQD2 (bottom). NubG is included as a negative control; no direct interaction between NET3C and IQD2 was observed after 3 days. **(B)** Growth assay of haploid yeast cells co-expressing the bait construct NET3C-Cub and the prey construct NubG-IQD2. KLCR1 and KLCR2 were included as a linker in yeast cells in the top and middle rows, respectively. Yeast cells were used at OD600 value of 1 (A) and 0.8 (B), and in dilutions of 1:10 and 1:100 on vector selective media (A, CSM_{-LW}, B, CSM_{-LWU}) and on interaction selective media (A, CSM_{-LWAHM}; B, $CSM_{-LWUAHM}$) with increasing Met concentrations. Growth was monitored after 4 days. The results indicate that NET3C only interacts with IQD2 in the presence of KLCR1 and KLCR2, suggesting that KLCR proteins facilitate the formation of a NET3C-KLCR-IQD complex. **(C)** The co-expression of RFP-NET3C, CFP-IQD2 and KLCR1-GFP in *N. benthamiana* suggests that the three proteins co-localized to microtubule like structures, and NET3C labeled EPCSs as puncta aligning along microtubules. **(D)** FRET-FLIM analysis of the interaction between NET3C and IQD2. The average fluorescence lifetime of GFP-NET3C was measured as 2.49 ± 0.01 ns when expressed alone, whereas RFP-IQD2 was only able to reduce the fluorescence lifetime of GFP-NET3C by 0.07 ns, to an average value of 2.42 ± 0.01 ns. This difference in fluorescence lifetime does not indicate a convincing interaction. **(E)** Putative model of NET3C-KLCRs-IQDs complex at the EPCSs. KLCRs interact with IQDs at the microtubules and may transiently associated with EPCSs and actin cytoskeleton through interacting with NET3C. **(F)** Diagram of interaction between IQDs, NET3C, KLCRs and VAP27-1. Blue solid lines indicate physical interactions which were confirmed using FRET-FLIM or yeast-two-hybrid. Dotted lines indicate co-localization or indirect interactions. **(G)** *N. benthamiana* cells co-expressed with CFP-HDEL and Tubulin-mCherry were used as a control in the analysis of ER morphology. **(H)** The morphology of the ER (as labelled by CFP-HDEL) is altered when RFP-NET3C is over-expressed. The average number of polygonal ER structures were increased. **(I)** The quantification of polygon numbers per micron. Asterisks indicate statistically significant differences from wild type (t-test, ***$p<0.001$). n=17 cells. **(J)** Schematic of NET3C in relation to the cortical ER network. Under control conditions, the expression of NET3C is low and the ER meshwork appears to be normal. However, over-expression of NET3C may cause more ER-PM contact sites resulting in more ER polygonal rings being produced. **(K-M)** KLCR1, NET3C and IQD2 form a protein complex and facilitates the association between the ER network and microtubules. Over-expression of both IQD2 and NET3C induces a rearrangement of ER network along the microtubules. Scale bar: 10 μm. See also Figures S2-S3.

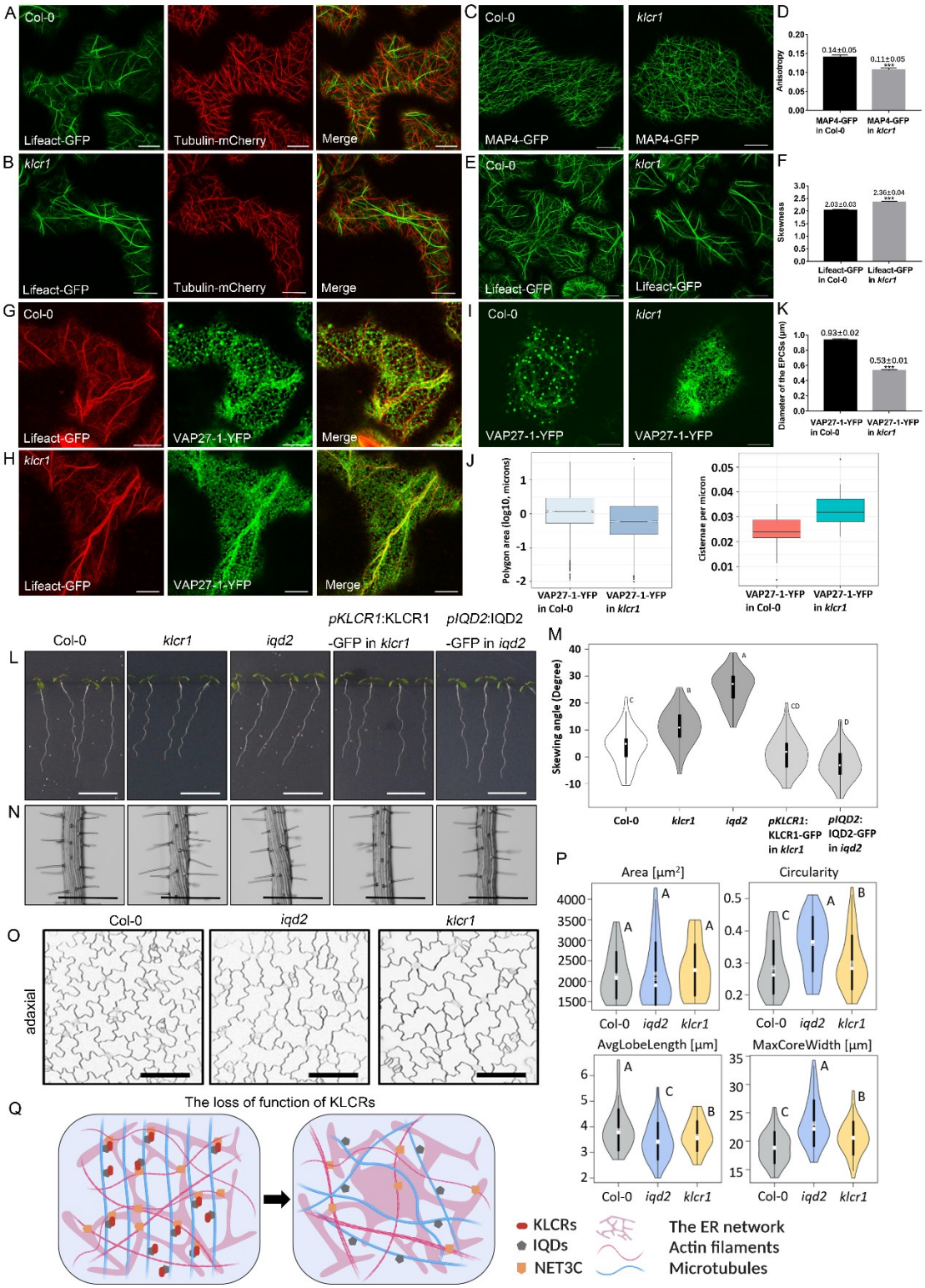

Figure 4. The loss of function mutants of KLCR1, NET3C and IQD2 are defective in pavement cell morphogenesis. (A-B) Representative images of cotyledon pavement cells co-expressing Lifeact-GFP and Tubulin-mCherry. The cytoskeleton network is disorganized in the *klcr1* mutants. **(C-D)** Representative images of cotyledon pavement cells expressing MAP4-GFP, quantitative analysis of cortical microtubule arrays suggested that the anisotropy of *klcr1* mutant was significantly reduced (0.11±0.05) in contrast to the wild type (0.14±0.05), suggesting the structure of microtubules are more disordered without KLCR1. Asterisks

indicate statistically significant differences from wild type (Student's t-test, ***p<0.001) **(E-F)** Representative images of cotyledon pavement cells expressing Lifeact-GFP, the average skewness value of actin filaments in wild type plants is observed to be 2.03±0.03, which was significantly smaller than the value in the same cells in *klcr1* plants (2.36±0.04). Asterisks indicate statistically significant differences from wild type (Student's t-test, ***p<0.001). **(G-H)** Representative images of cotyledon pavement cells co-expressing VAP27-1-YFP and Lifeact-GFP. Co-localization between thick ER stream and actin bundle can be clearly observed in *klcr1* mutant. **(I)-(J)** Representative images of cotyledon pavement cells expressing VAP27-1-YFP. The structure of ER network and EPCSs were affected in *klcr1* mutants. Asterisks indicate statistically significant differences from wild type (t-test, ***p<0.001). n=15 to 18 cells from 5 to 6 seedlings. **(L-M)** Phenotypes of 7-day-old Arabidopsis seedlings. Primary roots of *klcr1* and *iqd2* mutants slanted towards the left side as viewed from above the plates. The root epidermal cells of *klcr1* and *iqd2* showed left-handed helical arrangement when compared to wild type, whose root epidermal cells exhibited parallel arrangement. Expression of *pKLCR1*: KLCR1-GFP and *pIQD2*:IQD2-GFP in the *klcr1* and *iqd2* mutants was able to rescue the twisting root growth phenotype. Root skewing scale bars: 1 cm. Epidermal cell file rotation scale bars: 1 mm. **(N)** Root slanting angles of 7-day-old wild type and mutant seedlings grown vertically on agar plates. The different uppercase letters indicate the significance of p<0.001 by Tukey's Multiple Comparison Test. n=40 to 50 seedlings. **(O)** Pavement cell shape in cotyledon of 5-day-old seedlings. Inverted confocal images of the adaxial (top) side of cotyledons from wild type (Col-0) and *klcr1* and *iqd2* mutants stained with40 μM propidium iodide (PI). Scale bar: 100 μm. **(P)** Violin plots of value distributions of cell area, circularity, lobe length and maximum core width. Circles and crosses refer to medians and means; vertical black lines represent SD (thick line) and the 95% confidence interval (thin lines). The width of each violin represents the local distribution of feature values along the y axes. Different letters denote significant statistical differences. (p<0.01 by Kruskal-Wallis and Dunn posthoc test). **(Q)** The loss of function of KLCR1 affects the structure of the cytoskeleton and the ER network. See also Figure S4.

Star Method

RESOURCE AVAILABILITY

Lead Contact and materials availability

Further information and requests for resources and reagents should be directed to and will be fulfilled by the Lead Contact, Pengwei Wang (wangpengwei@mail.hzau.edu.cn).
Unique materials used in this study will be freely available.

Data and Code availability

This study did not generate/analyze any unique datasets/code.

EXPERIMENTAL MODEL AND SUBJECT DETAILS

The WT Columbia-0 (Col-0) was used in all experiments. The T-DNA insertion mutants and transgenic lines in these backgrounds as detailed in the Key Resources Table. Arabidopsis plants were grown under a 16h (22 ^{o}C) 8h (18^{o}C) light/dark photoperiod in a growth room

Method Details

Plant material and transformations

Arabidopsis Columbia Col-0 ecotype was used as the background line for the generation of stable transgenic plants using the Agrobacterium-mediated floral-dipping as described in [37]. Seeds were grown on 1/2 Murashige and Skoog (1/2 MS) agar in a growth chamber with a 16h (22 ^{o}C): 8h (18 ^{o}C), light: dark regime. For IQD related work that was performed in Halle, seeds were surface-sterilized with chlorine gas and plated on plates with Arabidopsis thaliana Salts (ATS) medium, 0.5 % (w/v) phyto agar (DuchefaBiochmie), 1 % (w/v) sucrose [38]. Agrobacterium-mediated transient transformation of *N. benthamiana* leaf epidermal cells was performed according to [39]. *N. benthamiana* plants were kept in a growth room with a 16h (25 ^{o}C): 8h (18 ^{o}C), light: dark regime.

Molecular cloning

GFP-IQD1, GFP-IQD2, GFP-IQD12, GFP-IQD22 and GFP-IQD25 were generated in a previous study [40]. The cDNAs of full-length KLCRs 1-3 and NET3A-C were amplified from total seedling cDNA using PCR, with the primers listed in Supplemental Table S1. The fluorescent fusion

proteins were cloned into various destination vectors using Gateway cloning system (Invitrogen). The destination vector of pK7WGR2 (N-terminal RFP), pMDC83-RFP (C-terminal RFP), pMDC83-GFP (C-terminal GFP), pMDC83-mCherry (C-terminal mCherry) and pK7WGC2 (N-terminal CFP) were used for making fluorescence protein fusions. The KLCR1 gene with its promoter sequence (about 2kb upstream of its start codon) were cloned into pMDC107 vector for the expression of GFP tagged KLCR1 under its native promoter.

Live cell imaging and FRET-FLIM

Transient transformed *N. benthamiana* leaves were imaged two days after infiltration using laser scanning confocal microscope (LSCM; Leica TCS SP5). Images were taken in multi-track mode with line switching when multi-fluorescence was used. In order to reduce the likelihood of observing spectral bleed-through artifacts, for the GFP/YFP combinations, GFP was excited at 458 nm and the emission was detected at 470-510 nm, while YFP was excited at 514 nm and the emission was detected at 550-580 nm. For CFP/YFP/RFP combinations, CFP was excited at 405 nm and detected at 450-490 nm, YFP was excited at 488 nm and detected at 510-550 nm and RFP was excited at 543 nm and detected at 590-650 nm. For CFP/GFP/RFP combinations, CFP was excited at 405 nm and detected at 450-490 nm, GFP was excited at 488 nm and detected at 510-550 nm and RFP was excited at 543 nm and detected at 590-650 nm [41].

Forster resonance energy transfer-fluorescence lifetime imaging microscopy (FRET-FLIM) experiments were performed using the Leica SP5 LSCM installed with a PicoQuant FLIM LSM upgrade kit. The data acquisition and analysis were performed using the PicoQuantSymPho Time 32 software. The lifetime of the GFP donor construct co-expressed with cytosolic RFP was measured as the negative control. All measurements were taken from whole-field images of cells expressing fluorophore fusion proteins at similar level, and at least 6 measurements were taken for each analysis.

Immunofluorescence

To performed the immunofluorescence study, root tips or cotyledons of 6 days old Arabidopsis were fixed in microtubule stabilizing buffer (MSB:50 mM PIPES pH 6.8, 5 mM EGTA pH 6.8, 5mM $MgSO_4$) containing 300 µM MBS, 0.01% Triton X-100, 4% paraformaldehyde (PFA) and 0.01% glutaraldehyde for 3 h at room temperature. After the fixation step, the samples were washed 3 times with MSB buffer containing 0.05% Triton X-100, 5 min for each wash. For root tips, the samples were then digested in 2% Driselase for 7 min and for cotyledons, samples

were freeze shattered as described by *Zhang et al.* (2013) [42] After that, the digested or shattered tissues were transferred into the freshly prepared permeabilization buffer (1×PBS buffer pH7.4 with 0.1% Triton X-100) and kept in it for 1h. Samples were then incubated in 2% BSA for 1h to prevent unspecific binding of antibodies. After that, samples were incubated in primary and secondary antibody for 3h or overnight at 4^{o}C. For double staining with KLCR1-GFP or GFP-IQD2 expressing cells, antibodies were diluted at 1:100 for NET3C which was described in our previous study [1] and 1:200 for GFP, followed by secondary antibody incubation with TRITC-conjugated against rabbit (Jackson ImmunoResearch) and FITC-conjugate against mouse (Jackson ImmunoResearch). After washing with 1 ×PBS buffer for 3 times, samples were mounted with Vectashield mounting media before imaging.

Transient transformation of Arabidopsis seedlings

Arabidopsis transient transformation was performed as described by *Marion et al*. (2006) [43]. Overnight culture of *A. tumefaciens* cells were collected and resuspended at the appropriate concentration (OD_{600}=2) in 4 ml of 5% sucrose containing 200 µM acetosyringone. To perform the infiltration, 4 days old Arabidopsis seedlings were soaked in the *Argrobacterium* solution, followed by applying vacuum (10 mmHg) twice for 1min. The seedlings were then transferred to a 1/2 MS agar plate and the plate was kept in a growth room for 4 days before imaging.

Yeast-two-hybrid and split ubiquitin assays

To perform an Y2H screen, the full length NET3C cDNA was cloned into pGBKT7 plasmid (Clontech, Palo Alto, CA, USA) using gateway (Invitrogen), to facilitate its expression as bait protein constructs. The Arabidopsis cDNA library (cloned into pGADT7 plasmid) used here is generated in a previous study. Yeast strains (AH109) transformed with the cDNA library were mixed with Y187 yeast strains that transformed with the bait construct. The mixed culture was poured onto solid YPDA (yeast peptone dextrose adenine) plates and incubated overnight at 30 ^{o}C. The mated cells were washed off the plates in 1/2YPDA liquid medium and selected on standard defined (SD) media lacking tryptophan, leucine, histidine and adenine plus 2.5 mM of 3-Amino-1.2.4-triazole (3-AT). Colonies that started to grow after 4-5 days of incubation were streaked onto identical SD media and grow for another 5 days at 30 ^{o}C. The colonies that could survive on the second selection media were used to inoculate liquid cultures. The plasmids were purified and sequenced using T7 promoter primer listed in Supplemental Table S1.

For direct one on one Y2H test, the coding sequences of NET3A, NET3B, NET3C and IQD2 were

amplified by PCR and cloned into the bait pDEST32 vector to create plasmids encoding NET3 and IQD2 protein fusions with the Gal4 DNA binding domain. Plasmids encoding fusions of Arabidopsis KLCRs with the Gal4 activation were constructed by PCR and insert mobilization into the prey pDEST22 vector. All plasmid constructs were verified by DNA sequencing. The bait and prey vectors to be tested for interaction of the fusion proteins were co-transformed into *Saccharomyces cerevisiae* strain PJ69-4a using the standard LiOAc method [44]. 10 µL of the yeast were spotted on plates with vector selective media DDO (double drop out media: SD/-Leucin/-Trpytophan) and were grown for 3 days at 29 °C. Two independent colonies of each transformation were inoculated in 1x TE buffer and incubated at 29 °C over night. On the next day OD_{600} was adjusted to 0.5 -1. 10, 10 µL of the colonies were spotted on DDO, interaction selective media (triple drop out media: SD/-Leucin/-Tryptophan/-Histidin) and interaction selective media with a strong stringency (quadrupole drop out media: SD/-Leucin/-Tryptophan/-Histidin/- Adenin). Pictures were taken 3 days after spotting. SD plates were prepared with 1.6 % (w/v) Bactoagar (AppliChem) and the SD media was obtained from TakaraBio.

For split ubiquitin assay, yeast strain THY.AP4 (: MATa; ade2−, his3−, leu2−, trp1−, ura3−; lexA::ADE2, lexA::HIS3, lexA::lacZ) was co-transformed with desired plasmid DNA using LiOAc/PEG method. 50 ml yeast culture with OD600 = 0.6 - 0.8 were harvested by centrifugation (5 min at 3500 rpm at RT) and the obtained pellet was washed with 20 ml sterile ddH2O. Subsequently yeast was washed with 2 ml 1x LiOAc and was centrifuged again. Pellet was resuspended in suitable amount 1x LiOAc (20 µl 1x LiOAc per transformation). Yeast cells were incubated for 30 min at RT. For one transformation 500 ng Plasmid DNA (per construct), 20 µl ssDNA (10 mg/ml), 70 µl PEG3350 (50 % (v/w), and 10 µl 10x LiOAc were mixed in a PCR tube and incubated for 30 min at 30 °C followed by heat shock at 42 °C for 15 min. Samples were centrifuged and supernatant was discarded. Pellet was dissolved in 60 µl ddH2O and plated onto CSM –Leu/-Trp. Yeast colonies were obtained after 2-3 days at 30 °C.

For the detection of interaction, a minimum of two independent pools (5-8 single colonies) were grown in 2 ml CSM –Leu/-Trp over night at 30 °C and 120 rpm. The following day OD600 was measured and all cultures were adjusted to OD600 = 1. Also 1:10 and a 1:100 dilutions were prepared. 5 µl per undiluted and diluted culture were spotted on selective media CSM –Leu/-Trp/-Ade/-His/-Ura containing different Methionine concentrations (see figure legends), and on CSM –Leu/-Trp as growth control. Growth was recorded daily.

ER morphology analysis

The structure of the ER was analyzed as described in [45]. In brief, after initial up-sampling of the images collected using confocal microscopy, the ER is segmented from the background by applying Otsu's method of automatic thresholding [46]. Any polygonal regions fully enclosed within the segmented ER are filled to produce a single mask of the segmented ER network visible in each image. Only features within this region are considered for further analysis. Cisternae are segmented from the ER network using an opening function followed by active contouring onto the underlying image intensity. If any cisternae are identified as having an area below 0.3 μm^2, they are discounted from further cisternae analysis as they considered to be punctae as described by *Sparkes et al*. (2009) [47]. The tubular network is subsequently enhanced using phase congruency methods [48], to limit potential breaks forming in the network caused by variable intensity along the length of ER tubules. This enhanced network is reduced to a single pixel wide skeleton running along the ridge of tubules. Polygonal regions are segmented from the negative of the combined tubule skeleton and identified cisternae.

Reverse genetics and plant developmental studies

The KLCR1 and IQD2 insertion lines, SAIL_335_B08 and GK_608F07-021865, were ordered form the Nottingham Arabidopsis Stock Center (NASC). Homozygosity was confirmed by PCR using gene specific primers, and a T-DNA specific primer. RT-PCR was performed to assess the full-length transcripts in *klcr1* and *iqd2*. The housekeeping gene that is expressed at specific level, Actin, was used as a control to ensure the amount of the cDNA template used for each reaction was identical. All primers used in this study are listed in Supplemental Table S1.

For root growth assay, *klcr1*, *iqd2* and Col-0 plants were grown vertically on 1/2 MS agar plates in a growth chamber for 7 days. The root slanting angles were measured using ImageJ software. For pavement cell morphology analysis of Col-0, *klcr1* and *iqd2*, seedlings were grown vertically on ATS [38] agar (0.5% w/v) plates in a growth chamber. The parameters of pavement cells were determined from 5 day after germination stained with 40 µM propidium iodide for 10 minutes in the dark. About 140 cells from 12 seedlings were taken from the adaxial site of the cotyledon (12 cells per seedling). For pavement cell morphology analysis of net3a/NET3C RNAi, 4-day-old seedlings were stained with 5 µM (N-(3-Triethylammoniumpropyl)-4-(6-(4-(Diethylamino) Phenyl) Hexatrienyl) Pyridinium Dibromide) (FM4-64 dye) for 30 minutes in the dark. 200 to 500 cells from 6 to 8 seedlings were used for analysis. Pictures were taken with Zeiss LSM700.Parameters of pavement cell area, perimeter, circularity, average lobe length and max core width were measured with the PaCeQuant program as described in [49].

To investigate the structure of cytoskeleton in klcr1 mutants, fluorescence protein tagged actin marker, Lifeact-GFP or microtubule marker MAP4-GFP were previously introduced by crossing into the klcr1 genetic background. The GFP-tagged cytoskeleton was visualized using CLSM. About 7-10 wild type or mutant seedlings were selected for analyzing. For each seedling, 5-10 regions were evaluated. Skewness of fluorescence intensity distribution (correlated with microfilament bundling because bundles exhibit brighter fluorescence) was determined using the ImageJ 64 plugins and macros from Higaki's laboratory [50]. The anisotrophy score was used to quantify the microtubule structure and the measurement was performed using the ImageJ 64 plug-in, Fibriltool [51].

QUANTIFICATION AND STATISTICAL ANALYSIS

Data were generally presented as means ± SEM (standard error of the mean). For box plots, data were presented as median (center line); upper and lower quartiles (box limits); interquartile range (whiskers); outliers (points). For violin plots, the elements correspond to circles and crosses represent medians and means; vertical thick black lines represent SD (standard deviation); thin black lines represent the 95% confidence interval; The width of each violin represent local distribution of feature values along the y axes. For bar charts, box plots and violin plots were graphed using Graphpad Prism, MATLAB and BoxPlotR (http://shiny.chemgrid.org/boxplotr/) respectively. The biological replicates were indicated in each figure legend. Specific descriptions of statistical tests are provided in the figure legends.

Reference

1. Wang, P., Hawkins, T.J., Richardson, C., Cummins, I., Deeks, M.J., Sparkes, I., Hawes, C., and Hussey, P.J.J.C.B. (2014). The Plant Cytoskeleton, NET3C, and VAP27 Mediate the Link between the Plasma Membrane and Endoplasmic Reticulum. *24*, 1397-1405.
2. Siao, W., Wang, P., Voigt, B., Hussey, P.J., and Baluska, F.J.J.o.E.B. (2016). Arabidopsis SYT1 maintains stability of cortical endoplasmic reticulum networks and VAP27-1-enriched endoplasmic reticulum–plasma membrane contact sites. *67*, 6161-6171.
3. Lee, E., Vanneste, S., Pérez-Sancho, J., Benitez-Fuente, F., Strelau, M., Macho, A.P., Botella, M.A., Friml, J., and Rosado, A. (2019). Ionic stress enhances ER-PM connectivity via phosphoinositide-associated SYT1 contact site expansion in Arabidopsis. Proc Natl Acad Sci U S A *116*, 1420-1429.
4. Ishikawa, K., Tamura, K., Ueda, H., Ito, Y., Nakano, A., Hara-Nishimura, I., and Shimada, T. (2018). Synaptotagmin-Associated Endoplasmic Reticulum-Plasma Membrane Contact Sites Are Localized to Immobile ER Tubules. Plant Physiol *178*, 641-653.
5. Lee, E., Vila Nova Santana, B., Samuels, E., Benitez-Fuente, F., Corsi, E., Botella, M.A., Perez-Sancho, J., Vanneste, S., Friml, J., Macho, A., et al. (2020). Rare earth elements induce cytoskeleton-dependent and PI4P-associated rearrangement of SYT1/SYT5 ER-PM contact site complexes in Arabidopsis. J Exp Bot.
6. McFarlane, H.E., Lee, E.K., van Bezouwen, L.S., Ross, B., Rosado, A., and Samuels, A.L. (2017). Multiscale Structural Analysis of Plant ER–PM Contact Sites. Plant and Cell Physiology *58*, 478-484.
7. Brault, M.L., Petit, J.D., Immel, F., Nicolas, W.J., Glavier, M., Brocard, L., Gaston, A., Fouché, M., Hawkins, T.J., Crowet, J.-M., et al. (2019). Multiple C2 domains and transmembrane region proteins (MCTPs) tether membranes at plasmodesmata. EMBO Rep *20*, e47182.
8. Wang, P., Richardson, C., Hawkins, T.J., Sparkes, I., Hawes, C., and Hussey, P.J. (2016). Plant VAP27 proteins: domain characterization, intracellular localization and role in plant development. New Phytologist *210*, 1311-1326.
9. Deeks, M.J., Calcutt, J.R., Ingle, E.K.S., Hawkins, T.J., Chapman, S., Richardson, A.C., Mentlak, D.A., Dixon, M.R., Cartwright, F., and Smertenko, A.J.C.B. (2012). A Superfamily of Actin-Binding Proteins at the Actin-Membrane Nexus of Higher Plants. *22*, 1595-1600.
10. Burstenbinder, K., Savchenko, T., Muller, J., Adamson, A.W., Stamm, G., Kwong, R.W., Zipp, B.J., Dinesh, D.C., and Abel, S.J.J.o.B.C. (2013). Arabidopsis Calmodulin-binding Protein IQ67-Domain 1 Localizes to Microtubules and Interacts with Kinesin Light Chain-related Protein-1. *288*, 1871-1882.
11. Liu, Z., Schneider, R., Kesten, C., Zhang, Y., Somssich, M., Zhang, Y., Fernie, A.R., and Persson, S.J.D.C. (2016). Cellulose-Microtubule Uncoupling Proteins Prevent Lateral Displacement of Microtubules during Cellulose Synthesis in Arabidopsis. *38*, 305-315.
12. Ganguly, A., Zhu, C., Chen, W., and Dixit, R. (2020). FRA1 Kinesin Modulates the Lateral Stability of Cortical Microtubules through Cellulose Synthase-Microtubule Uncoupling Proteins. The Plant cell *32*, 2508-2524.
13. Kriechbaumer, V., Botchway, S.W., Slade, S.E., Knox, K., Frigerio, L., Oparka, K., and Hawes, C. (2015). Reticulomics: Protein-Protein Interaction Studies

with Two Plasmodesmata-Localized Reticulon Family Proteins Identify Binding Partners Enriched at Plasmodesmata, Endoplasmic Reticulum, and the Plasma Membrane. Plant Physiol *169*, 1933-1945.

14. Burstenbinder, K., Moller, B., Plotner, R., Stamm, G., Hause, G., Mitra, D., and Abel, S.J.P.P. (2017). The IQD Family of Calmodulin-Binding Proteins Links Calcium Signaling to Microtubules, Membrane Subdomains, and the Nucleus. *173*, 1692-1708.
15. Liang, H., Zhang, Y., Martinez, P., Rasmussen, C.G., Xu, T., and Yang, Z.J.P.P. (2018). The Microtubule-Associated Protein IQ67 DOMAIN5 Modulates Microtubule Dynamics and Pavement Cell Shape. *177*, 1555-1568.
16. Mitra, D., Klemm, S., Kumari, P., Quegwer, J., Moller, B., Poeschl, Y., Pflug, P., Stamm, G., Abel, S., and Burstenbinder, K.J.J.o.E.B. (2019). Microtubule-associated protein IQ67 DOMAIN5 regulates morphogenesis of leaf pavement cells in Arabidopsis thaliana. *70*, 529-543.
17. Sugiyama, Y., Wakazaki, M., Toyooka, K., Fukuda, H., and Oda, Y. (2017). A Novel Plasma Membrane-Anchored Protein Regulates Xylem Cell-Wall Deposition through Microtubule-Dependent Lateral Inhibition of Rho GTPase Domains. Curr Biol *27*, 2522-2528.e2524.
18. Azimzadeh, J., Nacry, P., Christodoulidou, A., Drevensek, S., Camilleri, C., Amiour, N., Parcy, F., Pastuglia, M., and Bouchez, D.J.T.P.C. (2008). Arabidopsis TONNEAU1 Proteins Are Essential for Preprophase Band Formation and Interact with Centrin. *20*, 2146-2159.
19. Drevensek, S., Goussot, M., Duroc, Y., Christodoulidou, A., Steyaert, S., Schaefer, E., Duvernois, E., Grandjean, O., Vantard, M., and Bouchez, D.J.T.P.C. (2012). The Arabidopsis TRM1–TON1 Interaction Reveals a Recruitment Network Common to Plant Cortical Microtubule Arrays and Eukaryotic Centrosomes. *24*, 178-191.
20. Grefen, C., Obrdlik, P., and Harter, K.J.M.o.M.B. (2009). The determination of protein-protein interactions by the mating-based split-ubiquitin system (mbSUS). *479*, 217-233.
21. Hamada, T., Ueda, H., Kawase, T., and Hara-Nishimura, I. (2014). Microtubules contribute to tubule elongation and anchoring of endoplasmic reticulum, resulting in high network complexity in Arabidopsis. Plant physiology *166*, 1869-1876.
22. Sun, J., Zhang, M., Qi, X., Doyle, C., and Zheng, H. (2020). Armadillo-repeat kinesin1 interacts with Arabidopsis atlastin RHD3 to move ER with plus-end of microtubules. Nat Commun *11*, 5510.
23. Boudaoud, A., Burian, A., Borowskawykret, D., Uyttewaal, M., Wrzalik, R., Kwiatkowska, D., and Hamant, O.J.N.P. (2014). FibrilTool, an ImageJ plug-in to quantify fibrillar structures in raw microscopy images. *9*, 457-463.
24. Furutani, I., Watanabe, Y., Prieto, R., Masukawa, M., Suzuki, K., Naoi, K., Thitamadee, S., Shikanai, T., and Hashimoto, T.J.D. (2000). The SPIRAL genes are required for directional control of cell elongation in Aarabidopsis thaliana. *127*, 4443-4453.
25. Naoi, K., and Hashimoto, T.J.T.P.C. (2004). A Semidominant Mutation in an Arabidopsis Mitogen-Activated Protein Kinase Phosphatase-Like Gene Compromises Cortical Microtubule Organization. *16*, 1841-1853.
26. Yuen, C.Y.L., Pearlman, R., Silosuh, L., Hilson, P., Carroll, K.L., and Masson, P.H.J.P.P. (2003). WVD2 and WDL1 Modulate Helical Organ Growth and Anisotropic Cell Expansion in Arabidopsis. *131*, 493-506.

27. Moller, B., Poeschl, Y., Plotner, R., and Burstenbinder, K.J.P.P. (2017). PaCeQuant: A Tool for High-Throughput Quantification of Pavement Cell Shape Characteristics. *175*, 998-1017.
28. Facette, M.R., Park, Y., Sutimantanapi, D., Luo, A., Cartwright, H.N., Yang, B., Bennett, E.J., Sylvester, A.W., and Smith, L.G.J.N.p. (2015). The SCAR/WAVE complex polarizes PAN receptors and promotes division asymmetry in maize. *1*, 14024-14024.
29. Zhang, C., Mallery, E.L., and Szymanski, D.B.J.F.i.P.S. (2013). ARP2/3 localization in Arabidopsis leaf pavement cells: a diversity of intracellular pools and cytoskeletal interactions. *4*, 238-238.
30. Wang, P., Hawes, C., and Hussey, P.J.J.T.i.P.S. (2017). Plant endoplasmic reticulum–plasma membrane contact sites. *22*, 289-297.
31. Wang, P., Gao, E., and Hussey, P.J. (2020). Autophagosome Biogenesis in Plants: An Actin Cytoskeleton Perspective. Trends in plant science *25*, 850-858.
32. Giordano, F., Saheki, Y., Idevallhagren, O., Colombo, S.F., Pirruccello, M., Milosevic, I., Gracheva, E.O., Bagriantsev, S.N., Borgese, N., and De Camilli, P.J.C. (2013). PI(4,5)P2-Dependent and Ca2+-Regulated ER-PM Interactions Mediated by the Extended Synaptotagmins. *153*, 1494-1509.
33. Bayer, E.M., Sparkes, I., Vanneste, S., and Rosado, A.J.C.O.i.P.B. (2017). From shaping organelles to signalling platforms: the emerging functions of plant ER-PM contact sites. *40*, 89-96.
34. Basak, B., Krishnan, H., and Raghu, P.J.b. (2019). The lipid transfer function of RDGB at ER-PM contact sites is regulated by multiple interdomain interactions.
35. Ng, A.Y.E., Ng, A.Q.E., and Zhang, D.J.C.B. (2018). ER-PM Contacts Restrict Exocytic Sites for Polarized Morphogenesis. *28*, 146.
36. Wang, P., Pleskot, R., Zang, J., Winkler, J., Wang, J., Yperman, K., Zhang, T., Wang, K., Gong, J., Guan, Y., et al. (2019). Plant AtEH/Pan1 proteins drive autophagosome formation at ER-PM contact sites with actin and endocytic machinery. In Nat Commun, Volume 10. p. 5132.
37. Zhang, X., Henriques, R., Lin, S.-S., Niu, Q.-W., and Chua, N.-H. (2006). Agrobacterium-mediated transformation of Arabidopsis thaliana using the floral dip method. Nature protocols *1*, 641.
38. Lincoln, C., Britton, J.H., and Estelle, M. (1990). Growth and development of the axr1 mutants of Arabidopsis. The Plant Cell *2*, 1071-1080.
39. Sparkes, I.A., Runions, J., Kearns, A., and Hawes, C. (2006). Rapid, transient expression of fluorescent fusion proteins in tobacco plants and generation of stably transformed plants. Nature protocols *1*, 2019.
40. Bürstenbinder, K., Möller, B., Plotner, R., Stamm, G., Hause, G., Mitra, D., and Abel, S. (2017). The IQD Family of Calmodulin-Binding Proteins Links Calcium Signaling to Microtubules, Membrane Subdomains, and the Nucleus. Plant Physiol *173*, 1692-1708.
41. Wang, P., and Hussey, P.J. (2017). NETWORKED 3B: a novel protein in the actin cytoskeleton-endoplasmic reticulum interaction. Journal of experimental botany *68*, 1441-1450.
42. Zhang, C., Mallery, E.L., and Szymanski, D.B. (2013). ARP2/3 localization in Arabidopsis leaf pavement cells: a diversity of intracellular pools and cytoskeletal interactions. Frontiers in plant science *4*, 238.
43. Marion, J., Bach, L., Bellec, Y., Meyer, C., Gissot, L., and Faure, J.D. (2008). Systematic analysis of protein subcellular localization and interaction using high-throughput transient transformation of Arabidopsis seedlings. The Plant

journal : for cell and molecular biology *56*, 169-179.
44. Kim, J., Harter, K., and Theologis, A. (1997). Protein–protein interactions among the Aux/IAA proteins. Proceedings of the National Academy of Sciences *94*, 11786-11791.
45. Pain, C., Kriechbaumer, V., Kittelmann, M., Hawes, C., and Fricker, M. (2019). Quantitative analysis of plant ER architecture and dynamics. Nature communications *10*, 984.
46. Otsu, N. (1979). A threshold selection method from gray-level histograms. IEEE transactions on systems, man, and cybernetics *9*, 62-66.
47. Sparkes, I., Runions, J., Hawes, C., and Griffing, L. (2009). Movement and remodeling of the endoplasmic reticulum in nondividing cells of tobacco leaves. The Plant Cell *21*, 3937-3949.
48. Kovesi, P. (1999). Image features from phase congruency. Videre: Journal of computer vision research *1*, 1-26.
49. Möller, B., Poeschl, Y., Plötner, R., and Bürstenbinder, K. (2017). PaCeQuant: a tool for high-throughput quantification of pavement cell shape characteristics. Plant physiology *175*, 998-1017.
50. Higaki, T., Kutsuna, N., Sano, T., Kondo, N., and Hasezawa, S. (2010). Quantification and cluster analysis of actin cytoskeletal structures in plant cells: role of actin bundling in stomatal movement during diurnal cycles in Arabidopsis guard cells. The Plant journal : for cell and molecular biology *61*, 156-165.
51. Boudaoud, A., Burian, A., Borowska-Wykret, D., Uyttewaal, M., Wrzalik, R., Kwiatkowska, D., and Hamant, O. (2014). FibrilTool, an ImageJ plug-in to quantify fibrillar structures in raw microscopy images. Nature protocols *9*, 457-463.